Struct Multidisc Optim (2011) 43:405–417
DOI 10.1007/s00158-010-0570-2

RESEARCH PAPER

On the effect of self-penalization of piezoelectric composites in topology optimization

Fabian Wein · Manfred Kaltenbacher · Barbara Kaltenbacher · Günter Leugering · Eberhard Bänsch · Fabian Schury

Received: 29 January 2010 / Revised: 15 July 2010 / Accepted: 1 September 2010 / Published online: 23 September 2010

Abstract We investigate the occurrence of *self-penalization* in topology optimization problems for piezoceramic-mechanical composites. Our main goal is to give physical interpretations for this phenomenon, i.e., to study the question why for various problems intermediate material values are not optimal in the absence of explicit penalization of the pseudo densities. In order to investigate this effect numerical experiments for several static and/or dynamic actuator and sensor objective functions are performed and their respective results are compared. The objective functions are mean transduction, displacement, sound power, electric potential, electric energy, energy conversion and electric power.

F. Wein (✉) · G. Leugering · E. Bänsch · F. Schury
Department of Mathematics, University of Erlangen-Nuremberg, 91058 Erlangen, Germany
e-mail: fabian.wein@am.uni-erlangen.de

G. Leugering
e-mail: leugering@am.uni-erlangen.de

E. Bänsch
e-mail: baensch@am.uni-erlangen.de

F. Schury
e-mail: schury@am.uni-erlangen.de

M. Kaltenbacher
Department of Applied Mechatronics, Alps-Adriatic University Klagenfurt, Universitatsstrasse 65−67, Klagenfurt 9020, Austria
e-mail: manfred.kaltenbacher@uni-klu.ac.at

B. Kaltenbacher
Institute of Mathematics and Scientific Computing, University of Graz, Universitätsplatz 3, Graz 8010, Austria
e-mail: Barbara.Kaltenbacher@uni-graz.at

Keywords SIMP · Topology optimization · Piezoelectricity · Self-penalization

1 Introduction

The term *topology optimization* refers to a structural optimization task. For every point within the design domain it is determined by the *pseudo density* vector $\boldsymbol{\rho}$ if existence or non-existence of material is more advantageous with respect to a cost function.

This approach is termed the SIMP[1] method, albeit one uses this term for a whole family of methods that might differ significantly from the ''standard'' SIMP approach. We refer to our optimization also as SIMP, even when no penalization is used. The term *ersatz material approach* would be more appropriate but is not that commonly used.

SIMP, going back to Bendsøe (1989), is a well known technique, not only in academics but also in industry. The standard monograph for advanced SIMP optimization is Bendsøe and Sigmund (2003), which includes several extensions and applications and condenses a large set of experience.

Looking at compliance optimization problems, it is known that the optimal solution shows unphysical and not easily interpretable *intermediate* or *gray* material if there are no further measures taken.

To quantify the amount of intermediate material, a measure for *grayness* for the design vector $\boldsymbol{\rho}$ is defined as follows

$$g_{\text{gray}}(\boldsymbol{\rho}) = \int_{\Omega} 4 * (1 - \rho(\boldsymbol{x}))\rho(\boldsymbol{x}) d\boldsymbol{x}, \tag{1}$$

[1] Solid Isotropic Material with Penalization

which normalizes the maximum grayness to one for ''half grayness'', assuming $|\Omega| = 1$, see e.g., Sigmund (2007).

There are of course a lot of methods known, e. g. penalization and filtering, which get rid of these unwanted and difficult to interpret values.

However, when considering topology optimization in other contexts, the problems sometimes shows an intrinsic penalization or *self-penalization*, as it is called by Sigmund, and the resulting optimal solutions only show a small amount of grayness in the absence of penalization and/ or filtering and volume constraint. This effect appears to be first reported in Sigmund and Jensen (2003) for the optimization of band gaps.

To the authors' best knowledge, self-penalization of piezoelectric material has explicitly only been described by Rupp et al. (2009a, b). Dühring (2009) performed piezoelectric topology optimization without volume constraints and penalization but applied filtering. The authors mention the issue first in Wein et al. (2008, 2009a).

Piezoelectric topology optimization is a multiphysics problem with the pseudo density applied concurrently to three or four material properties. It started with Silva and Kikuchi (1999) where a homogenization approach has been used. SIMP optimization of piezoelectric materials has been done first in Kögl and Silva (2005). As we show in this paper some of the respective material effects are counteracting. There is an optimal pseudo density vector $\boldsymbol{\rho}^*$, where these counteracting effects are balanced in such a way that no grayness occurs and self-penalization is observed.

Optimizing for the piezoelectric *polarization*, self-penalization is known and analytically proven in Donoso and Bellido (2009), but polarization is not considered within this work.

We use a piezoelectric-mechanical transducer consisting of a square piezoceramic plate attached to an elastic plate as benchmark problem to discuss the topology optimization for several objective functions. The actuator objective functions are *mean transduction* as in Kögl and Silva (2005), *displacement* e.g., by the authors in Wein et al. (2009a) and *acoustic sound power* by the authors in Wein et al. (2009b). Furthermore, we investigate the sensor objective functions *electric potential* and *electric energy* e.g., by the authors Wein et al. (2009c), *energy conversion factor* applied in Zheng et al. (2008) and *electric power* on the basis of an external electrical circuit originating in Rupp et al. (2009b).

To ease the comparison of the optimizations, the static formulation of the objective functions is applied when it is possible. Note, that this has only limited practical use from an engineering point of view. This especially holds true for the sensor objective functions, where static operation is merely of academic interest. For the design of real world sensor applications *electric power* is of interest.

For most objective functions we observe strong to moderate self-penalization. Some objective functions exhibit vanishing piezoelectric material in the absence of a volume constraint. This effect is not due to rigid-body movement as the elastic plate provides support.

The paper is organized as follows: Section 2 motivates penalization, volume constraint and regularization based on the classical elasticity compliance problem. Section 3 provides the applied optimization framework. The setup of the investigated transducer is introduced in Section 4, the mathematical modeling is given in Section 5. Section 6 explains (static) piezoelectric self-penalization. We then present the objective functions for the numerical experiments in Section 7. The numerical results are given in Section 8. Lastly, Section 9 concludes with a summary. In the Appendix the material data is given.

2 Implications of classical compliance optimization

As a motivation for the need of penalization the common compliance problem in linear elasticity is recalled. The review paper Sigmund and Petersson (1998) gives a good insight.

A body with mechanical support is subject to an external load (force), modeled by linear elasticity and numerically solved via the finite element method. For each cell of the finite element mesh the density/stiffness can be controlled from full material to void material (e.g., air) via a scalar variable ρ_e (*pseudo density*). The finite set of ρ_e represents the design vector $\boldsymbol{\rho}$.

The compliance minimization problem then asks for a minimal displacement of the load points in the direction of the applied forces and the optimization problem is to find the optimal vector of pseudo densities $\boldsymbol{\rho}$. The solution to this problem is trivial: full material. When the design variables are defined from almost zero (void material) to one (full material) it is easy to limit the amount of available material (*volume constraint*). It can be shown that a unique solution exists for this problem (also known as *variable thickness sheet problem*) but most ρ_e will have intermediate values (*gray material*) while only the lower and upper bound of ρ_e has a direct physical interpretation.

A strategy is to penalize intermediate material and the method suggested in Bendsøe (1989) is now referred to as SIMP. However, penalization adds a new parameter p to the optimization problem, which has to be chosen and a new difficulty may arise with checkerboard like microstructures of the penalized solution. The reason is given by the poor numerical approximation property of low order finite elements (Diaz and Sigmund 1995). A common approach to prevent checkerboards is *sensitivity filtering* (Sigmund 1994), where the sensitivities of the objective function are

averaged over the neighborhood. However, a fixed neighborhood will result in different solutions for finer or coarser finite element meshes. This effect is called *mesh dependency* and is a hint to the non-existence of a solution. It has been resolved by Sigmund via a geometric filter radius r independent on the discretization (but dependent on the model).

With the term *SIMP* one generally assumes the application of the techniques described above and the method has proven to be very efficient. Nevertheless one should be aware that they imply the following issues:

- One does not solve any more the original compliance problem with its nice convex properties.
- The choice of penalization method, penalization parameter p, filter method and filter parameter r results in different optimal solutions. The problem is changed and the solution applies only to an ersatz problem.
- Sensitivity filtering disturbs the sensitivities and an external optimizer cannot stop on mathematical optimality criteria as the KKT-condition.
- A volume constraint has a practical meaning for compliance minimization (optimal stiffness/weight ratio). However, for other problems with a bounded optimal volume fraction, penalization would not work, if the constrained volume coincides with the optimal volume.

The mathematical optimization problem has been changed by adding penalization and volume constraint as the original solution is not desired due to grayness. Similarly some maximization problems show an undesired solution, if the optimizer removes the mechanical support. This leads to rigid-body movements resulting in very high objective values. A solution to this is to add compliance minimization to the objective function (as with *mean transduction* and *energy conversion factor*). While this ensures mechanical support of the solution the following issues arise:

- Compliance minimization (stiffness maximization) might counteract to the original objective function.
- By adding compliance a multicriteria optimization problem is formed which might require the choice of a weighting parameter.
- Compliance minimization leads to gray solutions, hence penalization and volume constraint might become necessary.

In conclusion, we can state that it is very beneficial to not be forced to take measures, which might change the problem drastically, to prevent the occurrence of grayness in the solution.

3 Optimization framework

The purpose of this section is to shortly introduce the mathematical aspect of topology optimization via the SIMP method. This chapter restricts itself to elasticity as the extension to piezoelectricity is straight forward (Section 5).

We restrict ourselves to the time-harmonic case with the static analysis as special case only. Therefore, complex variables have no explicit symbol. Furthermore, there is no difference in the notation of continuous and discrete variables. The notation for non-scalar properties is bold, e.g., all discrete solution vectors. Any variable explicitly dependent on the design variable has a tilde.

The pseudo density $\rho_{\min} \leq \rho_e \leq 1$ is introduced for each of the N elements of the optimization domain—yielding the optimization design vector $\boldsymbol{\rho} = (\rho_1 \ \cdots \ \rho_N)^T$. Via a generic interpolation function $\mu(\rho_e)$ the ersatz material elasticity tensor $[\widetilde{\boldsymbol{c}}] = \mu(\rho_e)[\boldsymbol{c}]$ and ersatz mass density $\widetilde{\rho}_{\mathrm{m}} = \rho_e \rho_{\mathrm{m}}$ is gained. It is common practice to use no interpolation function for the latter. A usual interpolation function for dynamic problems is RAMP (**R**ational **A**pproximation of **M**aterial **P**roperties) $\mu_{\mathrm{RAMP}}(\rho_e) = \frac{\rho_e}{1+p(1-\rho_e)}$ and the standard power law interpolation form $\mu_{\mathrm{power}}(\rho_e) = \rho_e^p$ for (quasi) static cases with the penalization parameter p.

The finite element method (FEM) then leads to the local finite element stiffness matrix $\widetilde{\boldsymbol{k}}_e = \mu(\rho_e)\boldsymbol{k}_e$ and mass matrix $\widetilde{\boldsymbol{m}}_e = \rho_e \boldsymbol{m}_e$.

Assuming a sinusoidal excitation, a Fourier transformation gives the steady state solution in the complex domain.[2] With the Rayleigh element damping matrix $\boldsymbol{c}_e = \alpha_{\mathrm{K}}\boldsymbol{k}_e + \alpha_{\mathrm{M}}\boldsymbol{m}_e$ the element matrices are assembled to the global system resulting in

$$\widetilde{\boldsymbol{S}}(\omega)\,\boldsymbol{u}(\omega) = \left(\widetilde{\boldsymbol{K}} + j\omega\widetilde{\boldsymbol{C}} - \omega^2\widetilde{\boldsymbol{M}}\right)\boldsymbol{u}(\omega) = \boldsymbol{f}(\omega), \tag{2}$$

or $\widetilde{\boldsymbol{K}}\,\boldsymbol{u} = \boldsymbol{f}$ in the static case. The solution $\boldsymbol{u}$ depends implicitly on $\boldsymbol{\rho}$ and a design independent load $\boldsymbol{f}$ is assumed for simplicity. In the following the time dependence is not denoted explicitly any more .

The following steps are taken from Jensen (2007a), see also Sigmund and Jensen (2003) for the first published application and Jensen (2007b) for more details.

Sensitivity analysis gives the gradient of an objective function $J_0(\boldsymbol{\rho}, \boldsymbol{u}_R, \boldsymbol{u}_I)$ where the solution vector is split into real and imaginary part. In the following the dependencies are skipped. Following the adjoint method two residuals are added:

$$J = J_0 + \boldsymbol{\lambda}_1^T\left(\widetilde{\boldsymbol{S}}\,\boldsymbol{u} - \boldsymbol{f}\right) + \boldsymbol{\lambda}_2^T\left(\widetilde{\boldsymbol{S}}^*\boldsymbol{u}^* - \boldsymbol{f}^*\right),$$

[2] With imaginary unit j and $\omega = 2\pi f$.

where $\boldsymbol{\lambda}_1$ and $\boldsymbol{\lambda}_2$ are fixed vectors, $\boldsymbol{\lambda}_2$ corresponding to the complex conjugate system. One can find $\boldsymbol{\lambda}_1 = \boldsymbol{\lambda}_2^*$ and the final gradient results in

$$\frac{\partial J}{\partial \rho_e} = \frac{\partial J_0}{\partial \rho_e} + 2\,\Re\left\{\boldsymbol{\lambda}_e^T \frac{\widetilde{\boldsymbol{S}}_e}{\partial \rho_e}\boldsymbol{u}_e\right\}, \tag{3}$$

where it is sufficient to operate within the local element data and $\boldsymbol{\lambda} = \boldsymbol{\lambda}_1$ solves the adjoint equation

$$\widetilde{\boldsymbol{S}}\,\boldsymbol{\lambda} \;=\; -\frac{1}{2}\left(\frac{\partial J_0}{\partial \boldsymbol{u}_R} - j\frac{\partial J_0}{\partial \boldsymbol{u}_I}\right). \tag{4}$$

As mentioned in Section 1, penalization in elasticity leads to checkerboard like structures, requiring regularization like the Sigmund filter

$$\frac{\widetilde{\boldsymbol{S}}_e}{\partial \rho_e} = \frac{\sum_i H_i \frac{\rho_i}{\rho_e}\frac{\partial \mu(\rho_e)}{\rho_e}\widetilde{\boldsymbol{S}}_e}{\sum_i H_i}$$

with the distance function $H_i = r_{\min} - \mathrm{dist}(e, i)$.

4 Investigated piezoelectric transducer

Our piezoelectric transducer consists of a thin piezoelectric patch attached to a thin elastic plate. The piezoelectric layer represents the design domain. The mechanical support is provided by the elastic layer, which is not subject to optimization.

In more detail, we use a square aluminum plate with a length of 50 mm and a thickness of 100 µm. This plate is covered with a piezoelectric ceramic layer (PZT-5A) 50 µm thick. The displacement of the upper edges of the plate is fixed in the x, y and z-direction. The electrodes on the upper and lower side of the ceramic patch and a glue layer are neglected in the physical model. A FEM simulation of the setup for the inverse piezoelectric effect is shown in Fig. 1.

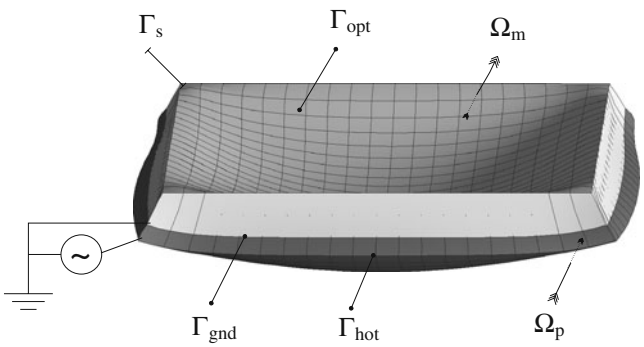

Fig. 1 The setup consists of an elastic plate Ω_m with simple support Γ_s and attached piezoelectric layer Ω_p. Electric excitation by the electrodes Γ_{gnd} and Γ_{hot} leads to bending

A full 3D formulation is used and we have confirmed numerically that our approach is correct for the thin structures using finite elements with quadratic ansatz functions.

The optimization problem is of 2 1/2 dimensions as the piezoceramic design space is discretized by a single finite element layer only.

The exact material properties are given in Appendix.

5 FEM formulation of the coupled problem

Kaltenbacher (2007) is used as reference for the following formulations, where the ersatz material properties are formed by applying the pseudo density without penalization

$$[\widetilde{\boldsymbol{c}}_e^E] = \rho_e\,[\boldsymbol{c}^E],\;\; [\widetilde{\boldsymbol{e}}_e] = \rho_e\,[\boldsymbol{e}\,],\;\; [\widetilde{\boldsymbol{\varepsilon}}_e^S] = \rho_e\,[\boldsymbol{\varepsilon}^S]. \tag{5}$$

The material law describing the piezoelectric effect is given (using Voigt notation) by

$$\begin{aligned}\boldsymbol{\sigma} &= [\widetilde{\boldsymbol{c}}^E]\,\boldsymbol{S} - [\widetilde{\boldsymbol{e}}\,]^T\boldsymbol{E},\\ \boldsymbol{D} &= [\widetilde{\boldsymbol{e}}\,]\,\boldsymbol{S} + [\widetilde{\boldsymbol{\varepsilon}}^S]\boldsymbol{E}.\end{aligned} \tag{6}$$

For the supporting mechanical plate Hooke's law is given by

$$\boldsymbol{\sigma} = [\,\boldsymbol{c}_m]\,\boldsymbol{S}. \tag{7}$$

We use the following quantities:

$\boldsymbol{E}$	electric field intensity
$\boldsymbol{D}$	electric displacement field
$\boldsymbol{\sigma}$	Cauchy stress tensor (6×1)
$\boldsymbol{S}$	linear strain tensor (6×1)
$[\widetilde{\boldsymbol{c}}^E]$	tensor of elastic moduli (6×6)
$[\widetilde{\boldsymbol{\varepsilon}}^S]$	tensor of dielectric permittivities (3×3)
$[\widetilde{\boldsymbol{e}}\,]$	tensor of piezoelectric moduli (3×6)
$[\boldsymbol{c}_m]$	tensor of elastic moduli (6×6)

$[\widetilde{\boldsymbol{c}}^E]$ is defined at constant electric field and $[\widetilde{\boldsymbol{\varepsilon}}^S]$ at constant mechanical strain.

5.1 System of PDEs

We denote the displacements $\boldsymbol{u} = (u_x\, u_y\, u_z)^T$ of the piezoelectric layer and the mechanical plate by $\boldsymbol{u}_p$ and $\boldsymbol{u}_m$,

respectively. Furthermore, we introduce the two differential operators

$$\mathscr{B} = \begin{pmatrix} \frac{\partial}{\partial x} & 0 & 0 & 0 & \frac{\partial}{\partial z} & \frac{\partial}{\partial y} \\ 0 & \frac{\partial}{\partial y} & 0 & \frac{\partial}{\partial z} & 0 & \frac{\partial}{\partial x} \\ 0 & 0 & \frac{\partial}{\partial z} & \frac{\partial}{\partial y} & \frac{\partial}{\partial x} & 0 \end{pmatrix}^T \quad \text{and}$$

$$\widetilde{\mathscr{B}} = \nabla = \begin{pmatrix} \frac{\partial}{\partial x} \\ \frac{\partial}{\partial y} \\ \frac{\partial}{\partial z} \end{pmatrix}. \tag{8}$$

Starting by using the piezoelectric setup as actuator, an electric potential ϕ_l (30 V) is applied to electrode $\boldsymbol{\Gamma}_\mathrm{hot}$ (18) and the strong formulation of the system of PDEs is given as:

Find

$$\boldsymbol{u}_\mathrm{p} : \overline{\Omega}_\mathrm{p} \to \mathbb{R}^3, \qquad \boldsymbol{u}_\mathrm{m} : \overline{\Omega}_\mathrm{m} \to \mathbb{R}^3, \qquad \phi : \overline{\Omega}_\mathrm{p} \to \mathbb{R}$$

fulfilling

$$\mathscr{B}^T \left([\widetilde{\boldsymbol{c}}_e^E] \mathscr{B} \boldsymbol{u}_\mathrm{p} + [\widetilde{\boldsymbol{e}}_e]^T \widetilde{\mathscr{B}} \phi \right) = 0 \quad \text{in } \Omega_\mathrm{p}, \tag{9}$$

$$\widetilde{\mathscr{B}}^T \left([\widetilde{\boldsymbol{e}}_e] \mathscr{B} \boldsymbol{u}_\mathrm{p} - [\widetilde{\boldsymbol{\varepsilon}}_e^S] \widetilde{\mathscr{B}} \phi \right) = 0 \quad \text{in } \Omega_\mathrm{p}, \tag{10}$$

$$\widetilde{\rho}_\mathrm{m} \ddot{\boldsymbol{u}} - \mathscr{B}^T [\boldsymbol{c}_m] \mathscr{B} \boldsymbol{u}_\mathrm{m} = 0 \quad \text{in } \Omega_\mathrm{m} \tag{11}$$

with the boundary conditions

$$\begin{aligned}
\boldsymbol{u}_\mathrm{m} &= \boldsymbol{0} && \text{on } \Gamma_\mathrm{s}, \\
\boldsymbol{n}_\mathrm{p}^T [\boldsymbol{\sigma}_\mathrm{p}] &= \boldsymbol{0} && \text{on } \partial\Omega_\mathrm{p} \setminus \Gamma_\mathrm{gnd}, && (12) \\
\boldsymbol{n}_\mathrm{m}^T [\boldsymbol{\sigma}_\mathrm{m}] &= \boldsymbol{0} && \text{on } \partial\Omega_\mathrm{m} \setminus (\Gamma_\mathrm{gnd} \cup \Gamma_\mathrm{s}), && (13) \\
\boldsymbol{n}_\mathrm{p}^T [\boldsymbol{\sigma}_\mathrm{p}] &= -\boldsymbol{n}_\mathrm{m}^T [\boldsymbol{\sigma}_\mathrm{m}] && \text{on } \Gamma_\mathrm{gnd}, && (14) \\
\boldsymbol{n}_\mathrm{p} &= -\boldsymbol{n}_\mathrm{m} && \text{on } \Gamma_\mathrm{gnd}, && (15) \\
\boldsymbol{u}_\mathrm{p} &= \boldsymbol{u}_\mathrm{m} && \text{on } \Gamma_\mathrm{gnd}, && (16) \\
\phi &= 0 && \text{on } \Gamma_\mathrm{gnd}, && (17) \\
\phi &= \phi_\mathrm{l} && \text{on } \Gamma_\mathrm{hot}, && (18) \\
\boldsymbol{n}_p^T \boldsymbol{D} &= 0 && \text{on } \partial\Omega_\mathrm{p} \setminus (\Gamma_\mathrm{hot} \cup \Gamma_\mathrm{gnd}). && (19)
\end{aligned}$$

The normal vectors $\boldsymbol{n}$ are extended by additional zero value where appropriate. Standard initial conditions are assumed.

5.1.1 Modeling of the direct piezoelectric effect

Using the system as a sensor, a traction (to be interpreted as pressure) $\boldsymbol{t}$ is applied

$$\boldsymbol{n}_\mathrm{m}^T [\boldsymbol{\sigma}_\mathrm{m}] = \boldsymbol{t} \text{ on } \Gamma_\mathrm{opt} \tag{20}$$

changing the boundary of (13) to

$$\boldsymbol{n}_\mathrm{m}^T [\boldsymbol{\sigma}_\mathrm{m}] = \boldsymbol{0} \text{ on } \partial\Omega_\mathrm{m} \setminus (\Gamma_\mathrm{gnd} \cup \Gamma_\mathrm{s} \cup \Gamma_\mathrm{opt}). \tag{21}$$

The electrodes Γ_gnd and Γ_hot represent equipotential surfaces. In the sensor case the inhomogeneous Dirichlet condition (18) for Γ_hot changes to a weak constraint (Q denotes the total charge on the loaded electrode)

$$\int_{\Gamma_\mathrm{hot}} \boldsymbol{n}_\mathrm{m}^T \boldsymbol{D} \, d\,\boldsymbol{\Gamma} = Q \qquad \text{on } \Gamma_\mathrm{hot}\,, \tag{22}$$

which reduces to a single degree of freedom on Γ_hot in the discrete system applying nodal constraint conditions.

5.2 Discrete FEM formulation

In Kaltenbacher et al. (2006) the weak system for an electrically excited piezoelectric system including the necessary test space compatible for the adjoint equation can be found. The element matrices $\widetilde{\boldsymbol{k}}_e^{\mathrm{uu}}$, $\widetilde{\boldsymbol{k}}_e^{\mathrm{u}\phi}$, $\widetilde{\boldsymbol{k}}_e^{\phi\phi}$ and $\widetilde{\boldsymbol{m}}_e^{\mathrm{uu}}$ are computed by the bilinear forms $\widetilde{k}_{pq}^{\mathrm{uu}}$, $\widetilde{k}_{pq}^{\mathrm{u}\phi}$, $\widetilde{k}_{pq}^{\phi\phi}$ and $\widetilde{m}_{pq}^{\mathrm{uu}}$ as

$$\begin{aligned}
\widetilde{k}_{pq}^{\mathrm{uu}} &= \rho_e \int_{\Omega_e} \mathscr{B}_p^T [\boldsymbol{c}^E] \mathscr{B}_q \, d\Omega, \\
\widetilde{k}_{pq}^{\mathrm{u}\phi} &= \rho_e \int_{\Omega_e} \mathscr{B}_p^T [\boldsymbol{e}\,] \widetilde{\mathscr{B}}_q \, d\Omega, \\
\widetilde{k}_{pq}^{\phi\phi} &= -\rho_e \int_{\Omega_e} \widetilde{\mathscr{B}}_p^T [\boldsymbol{\varepsilon}^S] \widetilde{\mathscr{B}}_q \, d\Omega, \\
\widetilde{m}_{pq}^{\phi\phi} &= \rho_e \int_{\Omega_e} \rho^\mathrm{m} \boldsymbol{N}_p^T \boldsymbol{N}_q \, d\Omega,
\end{aligned}$$

where $\boldsymbol{N}$ is the diagonal matrix of shape functions. The global finite element system with ersatz material for the piezoelectric layer results as

$$\begin{pmatrix} \boldsymbol{S}_{\mathrm{u_m u_m}} & \widetilde{\boldsymbol{K}}_{\mathrm{u_m u_p}} & \boldsymbol{0} \\ \widetilde{\boldsymbol{K}}_{\mathrm{u_m u_p}}^T & \widetilde{\boldsymbol{S}}_{\mathrm{u_p u_p}} & \widetilde{\boldsymbol{K}}_{\mathrm{u_p}\phi} \\ \boldsymbol{0} & \widetilde{\boldsymbol{K}}_{\mathrm{u_p}\phi}^T & \widetilde{\boldsymbol{K}}_{\phi\phi} \end{pmatrix} \begin{pmatrix} \boldsymbol{u}_\mathrm{m} \\ \boldsymbol{u}_\mathrm{p} \\ \boldsymbol{\phi} \end{pmatrix} = \begin{pmatrix} \boldsymbol{0} \\ \overline{\boldsymbol{f}} \\ \overline{\boldsymbol{q}} \end{pmatrix}. \tag{23}$$

Note, that we use bold symbols as in the discrete system all properties are large vectors or matrices.

Electrical (18) and mechanical (20) excitation contribute to the right hand-side vector as $\overline{\boldsymbol{q}}$ and $\overline{\boldsymbol{f}}$. A short form of (23) with

$$\widehat{\boldsymbol{u}} = (\boldsymbol{u}_\mathrm{m}\, \boldsymbol{u}_\mathrm{p}\, \boldsymbol{\phi})^T \tag{24}$$

is given as

$$\widetilde{\boldsymbol{S}}\, \widehat{\boldsymbol{u}} = \widehat{\boldsymbol{f}} \tag{25}$$

and for the static case as

$$\widetilde{\boldsymbol{K}}\, \widehat{\boldsymbol{u}} = \widehat{\boldsymbol{f}}. \tag{26}$$

Deriving the weak form of the adjoint equation shows, that for the actuator case, the inhomogeneous Dirichlet boundary condition (18) becomes a homogeneous Dirichlet boundary condition in (4).

6 Self-penalization of piezoelectric material

6.1 Self-penalization in elasticity

The optimal topology for compliance minimization is full material. Restricting the amount of available (ersatz) material by a volume constraint shows a smooth (*gray*) ersatz material distribution. There is no reason, why only full or void material should be advantageous. This is different for *mechanism synthesis* (Sigmund 1997), where the optimizer constructs mechanisms like force inverters, grippers, ... by the use of bars and hinges. While these sub-structures need to be of full material, void regions give space for movement. Nevertheless, regions of intermediate material will also appear.

This may change for dynamic problems. In Sigmund and Jensen (2003), which gives also the base for the sensitivity analysis in Section 3, neither penalization nor a volume constraint were required.

6.2 Balancing counteracting material effects

A major part of this work is the investigation of the mechanism resulting in piezoelectric self-penalization. For simplicity we restrict ourselves to the static situation. The inverse piezoelectric effect (actuator mode) is measured by the mechanical displacement (32) and the direct piezoelectric effect (sensor mode) is measured by the electric potential (37) as both properties are the solution of the physical model.

When we vary the pseudo density from void to full material, it is clear that the system depicted in Fig. 1 becomes stiffer with higher pseudo density, hence counteracting an actor application. For a sensor application the material laws (6) tell us that high stiffness, which means low bending/strain, results in low piezoelectric coupling and thus in a small sensor effect. On the other side it is clear for the piezoelectric coupling contribution that there is no actor or sensor effect at all for void material. Hence, lower or higher pseudo density have contrary effects and it is indeed the combination of these contrary effects which results in self-penalization as will be shown within this section. The electrostatic contribution cannot be seen directly.

Next we perform an unphysical gedankenexperiment. Consider the two plate system in Fig. 1 where each layer is discretized by finite elements. For the piezoelectric layer we reduce the vector of pseudo densities $\boldsymbol{\rho}$ to a scalar value ρ, effectively treating every element contribution with the same factor $\rho_e = \rho$. Furthermore, ρ is applied separately to the piezoelectric material properties, for example $[\widetilde{\boldsymbol{c}}_e^E] = \rho\,[\boldsymbol{c}^E]$, $[\widetilde{\boldsymbol{e}}_e] = [\boldsymbol{e}]$ and $[\widetilde{\boldsymbol{\varepsilon}}_e^S] = [\boldsymbol{\varepsilon}^S]$ to examine the stiffness contribution or $[\widetilde{\boldsymbol{c}}_e^E] = [\boldsymbol{c}^E]$, $[\widetilde{\boldsymbol{e}}_e] = \rho\,[\boldsymbol{e}]$ and $[\widetilde{\boldsymbol{\varepsilon}}_e^S] = [\boldsymbol{\varepsilon}^S]$ to examine the piezoelectric coupling.

Figure 2a visualizes the gedankenexperiment for the static actor. The displacement decreases with increasing pseudo density contribution to $[\boldsymbol{c}^E]$, denoted by *mech* due to higher stiffness . The piezoelectric coupling effect, denoted by *coupling* behaves linearly and the electrostatic contribution, denoted by *elec*, has no effect. Applying the pseudo density concurrently to all piezoelectric material properties, we get a superposition of the effects, which is clearly not a mere superposition of the graphs. This is denoted by *mech+coupling+elec*. Note, that coupling dominates stiffening in this example.

For the sensor case, depicted in Fig. 2b, all material properties contribute nonlinearly, the stiffness contribution is not even monotonous with a maximum displacement for pseudo density around 0.4. The electrostatic contribution dominates here, especially at the lower limit of the pseudo density, due to maximal bending.

Considering the range of feasible pseudo density between $\rho_{\min}$ and 1 in Fig. 2a and b the best response for the concurrent application of the design variable occurs at the bounds of the pseudo density. Hence no grayness appears and we observe self-penalization. Intermediate optimal density occurs when the balance of the superposition of the

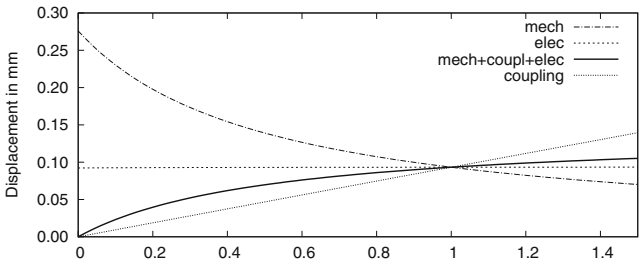

(a) Actuator mode with electric excitation by 30 V

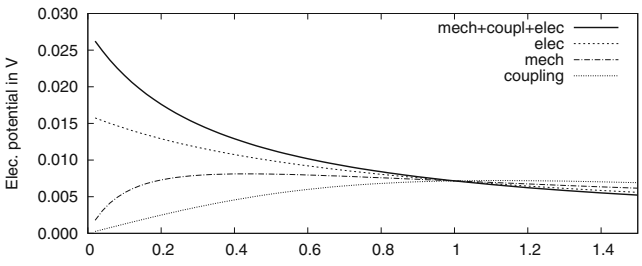

(b) Sensor mode with pressure excitation by 1 N/m^2

Fig. 2 In the sense of a gedankenexperiment, the design domain Ω_p is modeled by a single design variable ρ which is varied from $\rho_{\min}$ to $\rho_{\text{large}} > \rho_{\max}$. ρ is applied separately to $[\boldsymbol{c}^E]$, $[\boldsymbol{\varepsilon}^S]$, $[\boldsymbol{e}]$

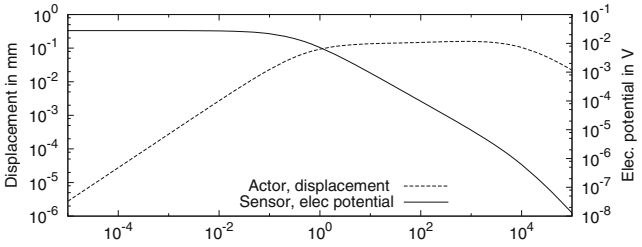

Fig. 3 Sensor and actuator modes for different ratio of plate and piezoelectric layer thickness applying extreme ρ

(a) No electrodes (b) With electrodes

Fig. 4 Electric potential induced by harmonic mechanical displacement to the system (Fig. 1). If there were no electrodes as in (**a**) local compression and expansion results in electric potential of opposite sign within Ω_p but also at the surfaces Γ_{gnd} and Γ_{hot}. With electrodes (**b**), the electric potential averages both on Γ_{gnd} and Γ_{hot} to zero

counteracting material effects does not result at the bounds of the pseudo density.

For the actor mode, there is no electrostatic contribution, only a (strictly) monotonous decreasing displacement for increasing ρ and a linear increasing displacement for the piezoelectric coupling due to the induced strain. Hence, the superposition of these effects is necessarily monotonous or convex.

The standard system in Fig. 1 represents just a single combination of possible geometries and materials. This can be overcome when, again in the sense of a gedankenexperiment, extreme values for the pseudo density are allowed. This is depicted in Fig. 3 for the concurrent application of $\rho \gg 1$ to all material properties. The response of the actor mode is indeed convex and a bounded optimal pseudo density $\rho_{\min} < \rho^* \rho_{\max}$ for a maximal displacement exists. For the sensor mode the numerical experiment in Fig. 3 shows a strictly monotonous decreasing electric potential. Hence, the maximal response corresponds with a minimal pseudo density which is unbounded.

Generalizing from the setup of the gedankenexperiment with a single design variable to multi design case $\rho_{\min} \leq \rho_e \leq 1$, we expect for the static electric potential (37) vanishing piezoelectric material as the optimum is unbounded. For the mechanical displacement (32) grayness might appear as the optimum is bounded. Both conclusions are numerically confirmed with the numerical results in Sections 8.4 and 8.2.

6.3 Balancing resonance and canceling strains

For dynamic topology optimization one might assume, that resonating structures will perform good, independent of the actual actor or sensor objective function. Indeed. this is not the case with piezoelectricity, as here *strain cancellation* might occure, especially for several structural resonance modes (Erturk et al. 2009). Figure 4 explaines the effect with a cut through the system in Fig. 1, the excitation actually is the result of an eigenfrequency analysis. No electric potential can be measuerd at the electrodes in sensor mode and in actor mode the vibrational pattern cannot be excited.

In Wein et al. (2009a) it is shown that the optimizer is able to generate close to resonance vibrational patterns by distributing full and void material to regions of opposite strains.

7 Objective functions

Within this section, we discuss the different objective functions used in Section 8.

7.1 Mean transduction

There exists a wide range of publications, where the *mean transduction* has been used. It can be applied to both the direct and inverse piezoelectric effect. We refer to Kögl and Silva (2005).

The mean transduction gives a measure for ''... the conversion of electrical into elastic energy and vice versa''. It is based on two load cases and choosing the load cases properly, the maximization of the transduction corresponds to the maximization of the displacement with respect to the load cases. Defining a static load case a as charge $Q_a \neq 0$ and $\boldsymbol{f}_a = \boldsymbol{0}$ and static case b as $\boldsymbol{f}_b \neq 0$ and $Q_b = 0$, the mean transduction computes (using the FE formulation according to (23)) as

$$J_{\text{transd}} = \boldsymbol{\phi}_b^T \widetilde{\boldsymbol{K}}_{u\phi}^T \boldsymbol{u}_a + \boldsymbol{\phi}_b^T \widetilde{\boldsymbol{K}}_{\phi\phi} \boldsymbol{\phi}_a. \tag{27}$$

The gradient can be derived from the two load cases without the need to solve an adjoint equation and is given with notation (25) as

$$\frac{\partial J_{\text{transd}}}{\partial \rho_e} = -\widehat{\boldsymbol{u}}_a^T \frac{\partial \widetilde{\boldsymbol{K}}}{\partial \rho_e} \widehat{\boldsymbol{u}}_b.$$

Note, that Q_a and $\boldsymbol{f}_b$ are design independent and therefore constant. We are not aware of a formulation of mean transduction with design dependent pressure and charge density.

In the original work, the whole domain is design domain and elastic compliance minimization is added to ''avoid the structure becoming overly flexible'' as

$$J = w \ln J_{\text{transd}} - (1-w) \ln J_{\text{mech}}; \quad 0 \le w \le 1, \tag{28}$$

requiring a volume constraint for the compliance minimization and penalization.

7.2 Displacement

The direct control of the displacement in linear elasticity is known as *mechanism synthesis* (Sigmund 1997) for the static case and *wave guiding* (Sigmund and Jensen 2003) in dynamics. A subset of the global solution vector $\widehat{\boldsymbol{u}}$ is chosen with a diagonal selection matrix $\boldsymbol{L}^{\text{u}}$ having ones and zeros such that the displacement of Γ_{opt} in Fig. 1 is maximized in z-direction. To differentiate from further selection matrices, the index denotes the selected property from the multiphysics vector $\widehat{\boldsymbol{u}}$. The objective function with $\widehat{\boldsymbol{u}}^*$ being the conjugate complex of $\widehat{\boldsymbol{u}}$ is given as

$$J_{\text{u}} = \widehat{\boldsymbol{u}}^T \boldsymbol{L}^{\text{u}} \widehat{\boldsymbol{u}}^* = \left\langle \boldsymbol{L}^{\text{u}} \widehat{\boldsymbol{u}}, \widehat{\boldsymbol{u}} \right\rangle.$$

To denote more clearly that the displacement $\boldsymbol{u}$ from $\widehat{\boldsymbol{u}}$ (24) is used in the formulation we write

$$J_{\text{u}} = \boldsymbol{u}^T \overline{\boldsymbol{L}^{\text{u}}} \boldsymbol{u}^* = \widehat{\boldsymbol{u}}^T \boldsymbol{L}^{\text{u}} \widehat{\boldsymbol{u}}^*, \tag{29}$$

where the bar in $\overline{\boldsymbol{L}^{\text{u}}}$ denotes a sub-matrix of $\boldsymbol{L}^{\text{u}}$. The gradient of (29) computes as

$$\frac{\partial J_{\text{u}}}{\partial \rho_e} = 2\,\Re\left\{ \boldsymbol{\lambda}^T \frac{\partial \widetilde{\boldsymbol{S}}}{\partial \rho_e} \widehat{\boldsymbol{u}} \right\}, \tag{30}$$

where the adjoint equation (4) becomes

$$\widetilde{\boldsymbol{S}}\, \boldsymbol{\lambda} = -\boldsymbol{L}^{\text{u}} \widehat{\boldsymbol{u}}^*. \tag{31}$$

Most structural resonance modes have perfect strain canceling. Hence, the implicit objective is to resemble such vibrational patterns without strain canceling or to generate additional vibration patterns, see Wein et al. (2009a). In the static case J_{u} reduces with the selection vector $\boldsymbol{l}^{\text{u}}$ to

$$J_{\text{u}}^{\text{st}} = \widehat{\boldsymbol{u}}^T \boldsymbol{l}^{\text{u}}, \tag{32}$$

and the gradient to $\boldsymbol{\lambda}^T \frac{\partial \widetilde{\boldsymbol{K}}}{\partial \rho_e} \widehat{\boldsymbol{u}}$ with the adjoint equation $\widetilde{\boldsymbol{K}}\, \boldsymbol{\lambda} = -\boldsymbol{l}^{\text{u}}$.

7.3 Sound power

The coupled acoustic problem is not covered in (23). It needs to be extended by the acoustic domain by including the Helmholtz equation

$$\frac{1}{c^2} \frac{\partial^2 \psi}{\partial t^2} - \Delta\, \psi = 0, \tag{33}$$

solving for the scalar acoustic potential ψ with c the speed of sound and the Laplace operator $\Delta = \frac{\partial^2}{\partial x_i^2} = \widetilde{\mathscr{B}}^T \widetilde{\mathscr{B}}$ with the gradient operator $\widetilde{\mathscr{B}}$ defined in (8). See Kaltenbacher (2007) for the transmission and interface conditions. The sound power P_{ac} over a surface Γ_{opt} is given as

$$P_{\text{ac}} = \frac{1}{2} \int_{\Gamma_{\text{opt}}} \Re\{p_{\text{a}}\, v_{\text{n}}^*\}\, d\Gamma, \tag{34}$$

with the complex sound pressure p_{a} and v_{n}^* the complex conjugate of the normal particle velocity. The linear system solves for $\widehat{\boldsymbol{u}}_\psi$ which includes the discrete solution vector $\boldsymbol{\psi}$ of scalar acoustic potentials in addition to $\widehat{\boldsymbol{u}}$ (24). In Wein et al. (2009b) the objective function

$$J_{\text{sound}} = \omega^2 \boldsymbol{\psi}^T \overline{\boldsymbol{L}^{\psi}}\, \boldsymbol{\psi}^* = \omega^2\, \widehat{\boldsymbol{u}}_\psi^T \boldsymbol{L}^{\psi}\, \widehat{\boldsymbol{u}}_\psi^* \tag{35}$$

has been applied under acoustic far field conditions and compared with $\omega^2\, J_{\text{u}}$, which can also be derived from P_{ac} under a more relaxed assumption. Many structural resonance modes represent acoustic short circuits so that the optimizer has to find new resonating patterns (including the handling of canceling strains).

7.4 Electrical potential

This sensor problem, utilizing the direct piezoelectric effect, optimizes analogously to the displacement (29) the electric potential ϕ via

$$J_\phi = \boldsymbol{\phi}^T \overline{\boldsymbol{L}^{\phi}}\, \boldsymbol{\phi}^* = \widehat{\boldsymbol{u}}^T \boldsymbol{L}^{\phi}\, \widehat{\boldsymbol{u}}^*. \tag{36}$$

The corresponding static formulation is

$$J_\phi^{\text{st}} = \boldsymbol{\phi}^T \overline{\boldsymbol{l}^{\phi}} = \widehat{\boldsymbol{u}}^T \boldsymbol{l}^{\phi} \tag{37}$$

As ϕ is a solution of the PDEs, this is a natural objective function in mathematical terms, but for engineering practice only of limited use (see numerical results). The system is excited by a pressure (as mechanical inhomogeneous Neumann boundary condition (20)) and Γ_{hot} has to fulfill (22). Hence, one just selects the master node (according to the implementation of the constraint condition) by $\boldsymbol{L}^{\phi}$ or $\boldsymbol{l}^{\phi}$, respectively.

7.5 Electric energy

The electrostatic energy is given as

$$J_{\text{elec}} = \frac{1}{2}\, \boldsymbol{\phi}^T \widetilde{\boldsymbol{K}}_{\phi\phi}\, \boldsymbol{\phi}. \tag{38}$$

The same boundary conditions are applied as in the case of J_ϕ. The gradient is given as

$$\frac{\partial J_{\text{elec}}}{\partial \rho_e} = \frac{1}{2}\, \boldsymbol{\phi}^T \frac{\partial \widetilde{\boldsymbol{K}}_{\phi\phi}}{\partial \rho_e} \boldsymbol{\phi} + \boldsymbol{\lambda}^T \frac{\partial \widetilde{\boldsymbol{S}}}{\partial \rho_e} \widehat{\boldsymbol{u}}, \tag{39}$$

where $\boldsymbol{\lambda}$ solves $\widetilde{\boldsymbol{S}}\,\boldsymbol{\lambda} = -\widetilde{\boldsymbol{K}}_{\phi\phi}\,\boldsymbol{\phi}$.

7.6 Energy conversion

Energy conversion has been used in the context of piezoelectric energy harvesting in Zheng et al. (2008) as

$$J_\eta = \frac{W_{\text{elec}}}{W_{\text{total}}} = \frac{J_{\text{elec}}}{J_{\text{elec}} + J_{\text{mech}}}, \tag{40}$$

with $J_{\text{mech}} = \frac{1}{2}\,\boldsymbol{u}^T\,\widetilde{\boldsymbol{K}}_{\text{uu}}\,\boldsymbol{u}$ (also known as compliance) analogously to (38). The model in the original paper is a cantilever with a static force applied to the tip. The whole domain is design domain and penalization and a volume constraint is used. The difference of J_{elec} against J_η in the context of energy harvesting is subtle. For scenarios with vibrational excitation via prescribed displacements the available mechanical energy can be considered large compared to the output electric energy. What is indeed interesting is a property of J_η described in Weller (2009). Maximizing J_η involves the minimization of the compliance J_{mech}. Weller showed that the optimizer may even sacrifice J_{elec} for the sake of stiffer material. So J_η implicitly includes a stiffening part with the same effect as the explicit stiffening in the original mean transduction formulation (28) which is crucial when the whole domain is design domain.

7.7 Electric power

J_ϕ, J_{elec} and J_η share the problem, that an external electric circuit detunes the resonance frequency of the system. This is described in Rupp et al. (2009b), where an external electrical circuit is attached to the system, which can even be subject to optimization. For the discussion below we restrict ourselves to a given external Ohmic resistance R. The objective function

$$J_{\text{power}} = \frac{1}{2R}\boldsymbol{\phi}^T\overline{\boldsymbol{L}^\phi}\,\boldsymbol{\phi}^* \tag{41}$$

is similar to J_ϕ (36), the difference is within the algebraic system $\widetilde{\boldsymbol{S}}_{\text{R}}$, where the resistor R is included (Wang et al. 1999) between the electrode nodes ϕ_{gnd} and ϕ_{hot} as

$$-j\omega\frac{1}{\omega^2 R}\begin{pmatrix}+1 & -1\\ -1 & +1\end{pmatrix}\begin{pmatrix}\phi_{\text{hot}}\\ \phi_{\text{gnd}}\end{pmatrix} = \begin{pmatrix}0\\ 0\end{pmatrix}. \tag{42}$$

8 Numerical results

In this section we discuss the optimization results of our setup consisting of the aluminum plate with a piezoelectric layer (see Fig. 1). The design domain is restricted to the piezoelectric layer and we perform the optimization for the different objection functions as discussed in the previous section.

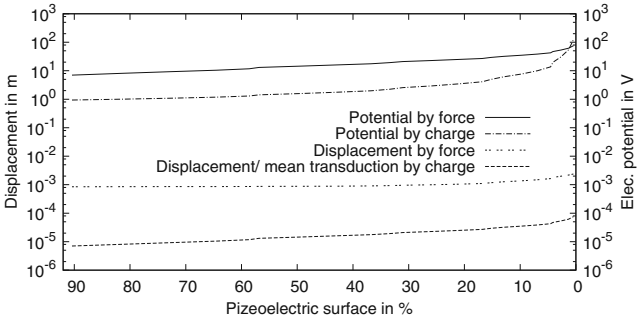

Fig. 5 Load cases *a* (electric charge) and *b* (nodal force) for the mean transduction J_{transd} (27) applied to a set of models with different sizes of Ω_p

8.1 Mean transduction

We observe a slow convergence for J_{transd} (27) towards a vanishing piezoelectric patch. This means that the optimizer produces a circular and centered patch with gradually decreasing radius. At the end a cluster of just a few non-void elements are left with densities close to void (ρ_{min}).

In order to validate this result, we perform a parameter study on a set of models, where the area of the piezoelectric layer becomes increasingly smaller. No void ersatz material is applied but different geometries. Two load cases (electric charge of 1 µC and nodal force of 1 N in z-direction at the plate center) are applied. Figure 5 shows, that for load case *a* with a constant electrical charge, displacement and electric potential increase due to an increase of the charge density (unbounded in the limit). Load case *b* with a force applied to the center, shows similar to Fig. 2b an increase of displacement and potential due to less stiffening (bounded). The mean transduction J_{transd} value coincides by definition with the displacement for the charge load case.

It needs to be emphasized, that we did not investigate mean transduction in conjunction with additional objective functions as it is done in literature. Self-penalization cannot arise in the case of vanishing material for the unconstrained problem.

8.2 Displacement

For the static case we use (32) as objective function and vary the thickness of the supporting plate Ω_{m} from 15 µm to 200 µm. Figure 6 displays the obtained optimal volumes and the corresponding grayness. The grayness is extremely low for most thickness relations with $g_{\text{gray}} \leq 0.02$ with an exception for a plate thickness around 40 µm (Fig. 6b). The volume fraction varies within 60−70% over the different thickness ratios.

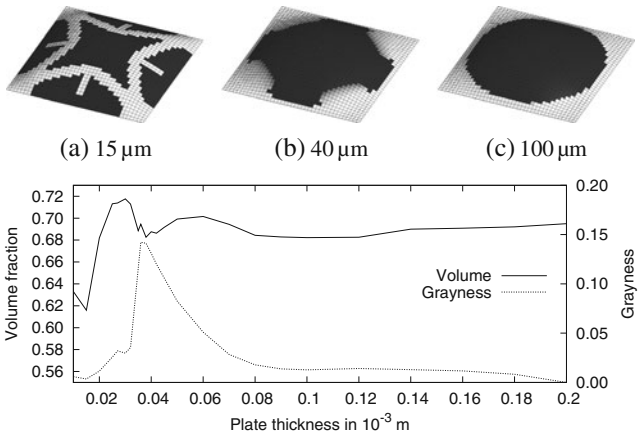

(d) Static displacement with varying thickness ratios

Fig. 6 Static displacement maximization by $J_{\mathrm{u}}^{\mathrm{st}}$ (32) for different elastic plate thicknesses

For the dynamic case, we use (29) as objective function and perform optimizations for several hundred single-frequencies in the range of 20−2,300 Hz. Here, the resulting structures have volume fractions from ≈40−100% as shown in Fig. 7. The difficulty for the optimizer is to balance the vibrational patterns between resonance and strain cancellation (Wein et al. 2009a) with varying success from frequency to frequency—explaining the discontinuity of the grayness in Fig. 7. Nevertheless the grayness if for all cases below 0.1.

At least for the considered models distinct self-penalization can be observed for both static and dynamic case. It shall be noted, that for the same objective function but within elasticity this has been observed in Sigmund and Jensen (2003).

8.3 Sound power

Optimizing for the sound power J_{sound} (35) requires the optimizer to balance resonance, compensation of canceling strains and acoustic short circuits. For a frequency range,

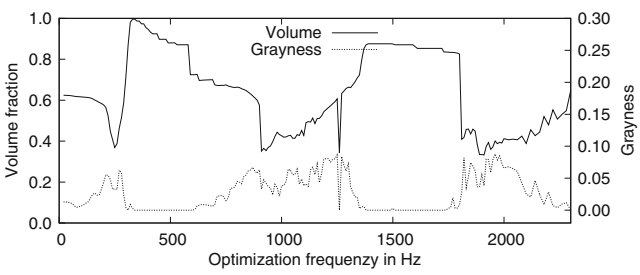

Fig. 7 Dynamic displacement maximization by J_{u} (29) applied for several hundred mono-frequency optimizations, taken from Wein et al. (2009a)

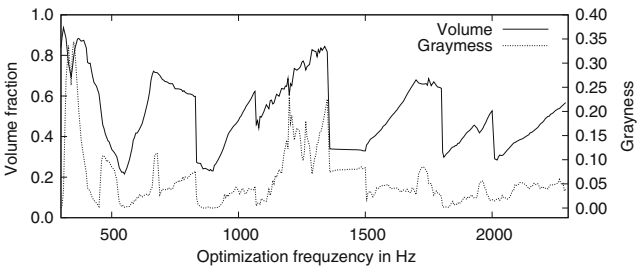

Fig. 8 Volume fraction and grayness optimizing for the sound power J_{sound} (35) taken from Wein et al. (2009b)

where acoustic far field conditions hold, the volume fraction and grayness are shown in Fig. 8. The optimal volumes range from 20−90%. In addition to Wein et al. (2009b) we did not start from full material but from a configuration deduced from the displacements of a structural eigenfrequency analysis. Compared to dynamic displacement maximization resonance could be generated for almost all frequencies—resulting in moderate self-penalization with grayness below 0.1 for most frequencies.

8.4 Electric potential

The sensor problems are excited by mechanical pressure of 1 N/m^2. The optimization problems for the electric potential ϕ in J_ϕ (36) and J_ϕ^{st} (37) are with respect to the mathematical structure identical to the displacement optimization problems (29) and (32).

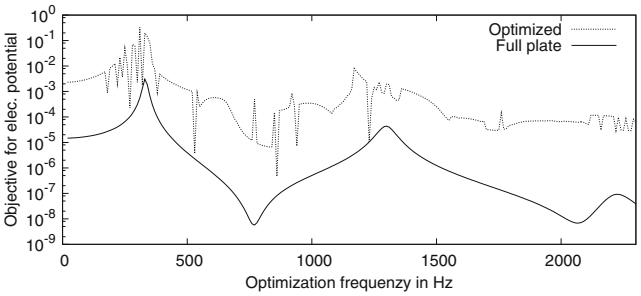

(a) Optimization for electric potential for varying excitation frequencies

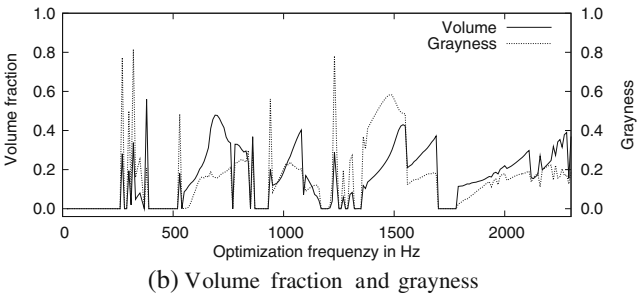

(b) Volume fraction and grayness

Fig. 9 Several hundred mono-frequent optimizations for dynamic potential J_ϕ as objective function. **a** Shows that several optimizations failed

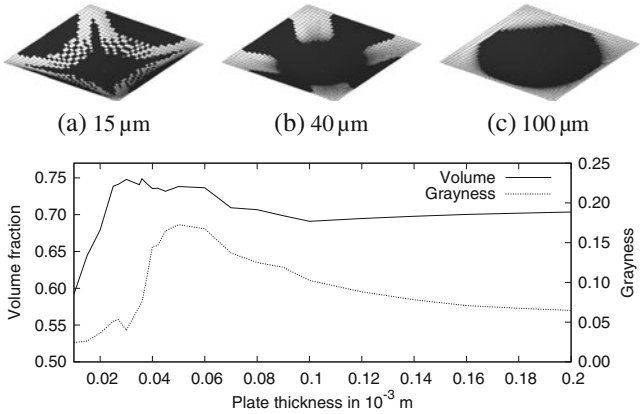

(a) 15 µm (b) 40 µm (c) 100 µm

(d) Static electric energy with varying thickness ratios

Fig. 10 Electrostatic energy maximization by J_{elec} (38) for different elastic plate thicknesses

For J_ϕ^{st} the optimizer removes the piezoelectric material as in the case of the mean transduction (see also Fig. 2b obtained by our simple numerical experiment). Lowest stiffness results in maximal strain which couples to the highest electric field, see (6).

In the dynamic case, we use J_ϕ as the objective function. Here, we observe that for the quasi-static excitation frequencies the same effect of vanishing material occurs. The performed dynamic optimization appears to be not very robust (Fig. 9a) and at least for the performed numerical experiments one cannot speak of self-penalization for electric potential maximization.

For a real-world experiment it would be difficult to measure the high potential of the resulting vanishing topology as the electric charge is also vanishing.

8.5 Electrostatic energy

Using the electrostatic energy J_{elec} (38) includes the material itself in the objective function and varying plate thickness results in volume fractions from 60−75% (Fig. 10d). Interesting is the occurrence of a checkerboard structure for very thin plates (Fig. 10a). This has not been observed for any other objective function. Self-penalization is moderate.

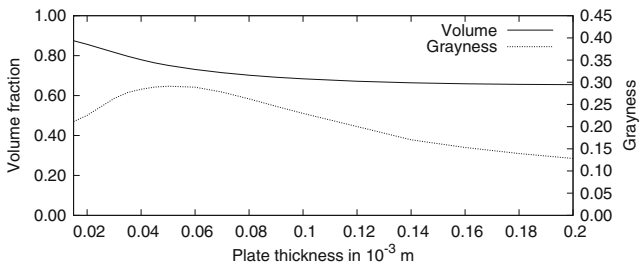

Fig. 11 Static energy conversion J_η for varying supporting plate thickness

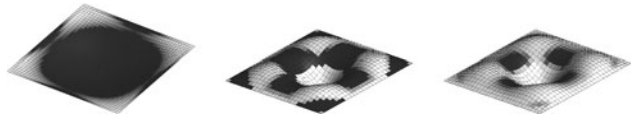

(a) J for 20 µm plate (b) J_{power}, R=100 Ω (c) J_{power} R=1000 Ω

Fig. 12 **a** Shows the optimization result for static energy conversion J_η (40) for a supporting plate thickness of 20 µm. **b**, **c** Show the optimization results for electric power J_{power} (41) at 1,500 Hz with external resistor R = 100 Ω and R = 1,000 Ω, respectively

8.6 Energy conversion

The energy conversion J_η (40) adds a compliance minimization problem to the pure electrical energy (38) maximization. The additional stiffening results in higher volumes (65−87%) and significantly more grayness (0.13−0.30). However, it has also a regulating effect and the obtained optimal solutions vary smoothly by the plate thickness ratio (Fig. 11). In Fig. 12a, we can observe the additional stiffening effect for a thin supporting plate of 20 µm.

8.7 Electric power

The optimization results for electric power J_{power} (41) significantly differs from the equivalent objective formulation J_ϕ, which is due to the different linear system matrix $\widetilde{\boldsymbol{S}}_{\text{R}}$ instead of $\widetilde{\boldsymbol{S}}$. There is no more vanishing piezoelectric material and the volume fractions result in the range of

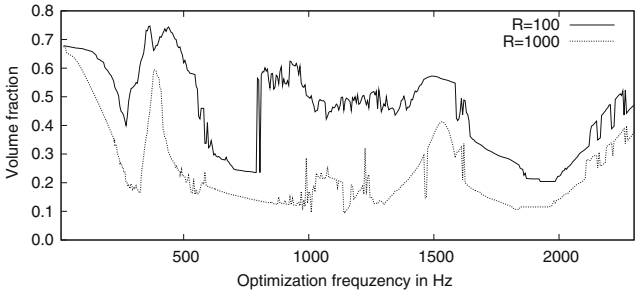

(a) Volume fractions for dynamic J_{power}

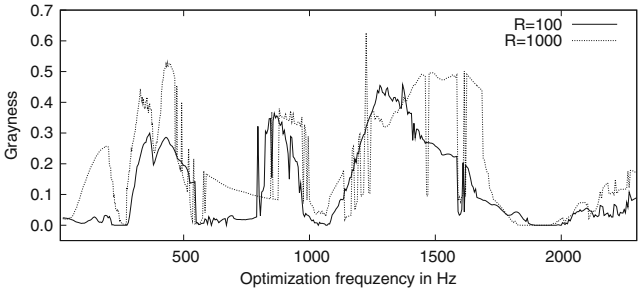

(b) Grayness for dynamic J_{power}

Fig. 13 Several hundred mono-frequency optimizations for the electric power J_{power} for fixed external resistors R = 100 Ω and R = 1,000 Ω. Resulting topologies for 1,500 Hz are shown in Fig. 12b and c

15−75%. Self-penalization depends on the external resistor and occurs only for certain frequency regions. So the general effect of piezoelectric self-penalization as reported in Rupp et al. (2009b) cannot be confirmed strictly. But while topology optimization there has also been performed for a constant external resistor, the major part and the conclusions refer to the concurrent optimization of the circuit. This is reported to significantly increase the optimization result and might also lead to stronger self-penalization Fig. 13.

9 Conclusions

For our investigations of a piezoelectric-mechanical compound we have demonstrated topology optimization based on the SIMP method of the piezoceramic layer without any restrictions. We have investigated several sensor and actuator objective functions in static and/or time harmonic formulation. For the static investigations we have varied the ratio of the thickness of the supporting elastic plate and piezoceramic layer (the latter kept constant). For time-harmonic experiments several hundred mono-frequency optimizations in the range up to several eigenfrequencies are performed. The resulting grayness measured by (1) and the volume fraction are observed.

From the numerical experiments we can clearly conclude a distinct self-penalization in the case of displacement maximization both for the static and dynamic case. Strong to moderate self-penalization could be observed for acoustic sound pressure maximization and a bit less for energy conversion and electric power maximization (at constant external Ohmic resistor). Furthermore, the two static objective functions—mean transduction and electric potential—resulted in vanishing piezoelectric material.

For dynamic optimization the obtained optimization result can have a strong dependence on initial design and/or excitation frequency. We observed that the self-penalizing effect is stronger for better final objective values.

For real world piezoelectric sensor and actuator design, applying explicit grayness penalization might then be necessary when the implicit self-penalization is not strong or reliable enough. There exists a wide range of methods, e.g., applying (1) as constraint as suggested e.g., in Stainko (2006) or black-and-white filters (Sigmund 2007). But this is outside the scope of this investigation.

Acknowledgments The authors gratefully acknowledge the funding of the German Research Council (DFG) by the DFG Priority Program 1253 'Optimization with Partial Differential Equations' through grants DFG06-381 and partially support within the framework of its 'Excellence Initiative' for the Cluster of Excellence 'Engineering of Advanced Materials' at the University of Erlangen-Nuremberg.

The authors would like to thank the anonymous reviewers for the helpful comments.

Appendix: Material properties

The applied piezoelectric material is lead zirconate titanate PZT-5A with the following properties (in Voigt notation): mass density 7.75025 kg/m^3, damping $\tan\delta = 0.015$ at 1,000 Hz, stiffness in GPa $c^E_{11} = c^E_{22} = 126$, $c^E_{13} = 79.5$, $c^E_{23} = c^E_{22} = 84.1$, $c^E_{44} = c^E_{55} = c^E_{66} = 23$, coupling in N/C $e_{15} = e_{24} = 17$, $e_{31} = e_{32} = -6.5$, $e_{33} = 23.3$, permittivity in 10^{-8} F/m $\varepsilon^S_{11} = \varepsilon^S_{22} = 1.51$, $\varepsilon^S_{33} = 1.27$.

The supporting aluminum plate has the following isotropic properties: Poisson's ratio $\nu = 0.34$, Young's modulus $E = 70.7$ GPa, mass density 2.7 kg/m^3, damping $\tan\delta = 0.03$ at 1,000 Hz.

For an accurate simulation model it might be necessary to determine the piezoelectric coupling coefficients by inverse methods as in Rupitsch and Lerch (2009).

References

Bendsøe MP (1989) Optimal shape design as a material distribution problem. Struct Multidisc Optim 1:193−202

Bendsøe MP, Sigmund O (2003) Topology optimization: theory, method and applications, 2nd edn. Springer

Diaz AR, Sigmund O (1995) Checkerboard patterns in layout optimization. Struct Multidisc Optim 10:40−45

Donoso A, Bellido J (2009) Systematic design of distributed piezoelectric modal sensors/actuators for rectangular plates by optimizing the polarization profile. Struct Multidisc Optim 38(4):347−356

Dühring MB (2009) Design of acousto-optical devices by topology optimization. In: Proceedings WCSMO-08, 1−5 June 2009. Lisbon, Portugal

Erturk A, Tarazaga P, Farmer J, Inman D (2009) Effect of strain nodes and electrode configuration on piezoelectric energy harvesting from cantilevered beams. Vibr Acoust 131(1):011010 (11 pages). doi:10.1115/1.2981094

Jensen JS (2007a) A note on sensitivity analysis of linear dynamic systems with harmonic excitation. Handout at DCAMM Advanced School, 20−26 June 2007 at DTU in Lyngby, Denmark

Jensen JS (2007b) Topology optimization of dynamics problems with Padé approximants. Int J Numer Methods Eng 72:1605−1630

Kaltenbacher M (2007) Numerical simulation of mechatronic sensors and actuators, 2nd edn. Springer, Berlin

Kaltenbacher B, Lahmer T, Mohr M, Kaltenbacher M (2006) PDE based determination of piezoelectric material tensors. Eur J Appl Math 17:383−416

Kögl M, Silva ECN (2005) Topology optimization of smart structures: design of piezoelectric plate and shell actuators. Smart Mater Struct 14(2):387−399

Rupitsch SJ, Lerch R (2009) Inverse method to estimate material parameters for piezoceramic disc actuators. Appl Phys A, Mater Sci Process 97(4):735−740

Rupp CJ, Evgrafov A, Dunn ML, Maute K (2009a) Topology optimization of piezoelectric energy harvesting structures and circuits. In: Proceedings WCSMO-08, 1−5 June 2009. Lisbon, Portugal

Rupp CJ, Evgrafov A, Maute K, Dunn ML (2009b) Design of piezoelectric energy harvesting systems: a topology optimization approach based on multilayer plates and shells. J Intel Mat Syst Str 20(16):1923−1939

Sigmund O (1994) Design of material structures using topology optimization. PhD thesis, Department of Solid Mechanics, Technical University of Denmark

Sigmund O (1997) On the design of compliant mechanisms using topology optimization. Mech Struct Mach 25(4):493−524

Sigmund O (2007) Morphology-based black and white filters for topology optimization. Struct Multidisc Optim 33(4):401−424

Sigmund O, Jensen JS (2003) Systematic design of phononic band-gap materials and structures by topology optimization. Philos Trans—Royal Soc, Math Phys Eng Sci 361(1806):1001−1019

Sigmund O, Petersson J (1998) Numerical instabilities in topology optimization: a survey on procedures dealing with checkerboards, mesh-dependencies and local minima. Struct Multidisc Optim 16:68−75

Silva ECN, Kikuchi N (1999) Design of piezoelectric transducers using topology optimization. Smart Mater Struct 8(3):350−364

Stainko R (2006) An adaptive multilevel approach to the minimal compliance problem in topology optimization. Commun Numer Methods Eng 22(2):109−118

Wang J, Ostergaard D, Inc A, Canonsburg P (1999) A finite element-electric circuit coupled simulation method forpiezoelectric transducer. In: Proceedings IEEE ultrasonics symposium, vol 2

Wein F, Kaltenbacher M, Schury F, Leugering G, Bänsch E (2008) Topology optimization of piezoelectric actuators using the SIMP method. In: Proceedings OIPE, 14−16 September 2009. TU Ilmenau, Germany, pp 46−47

Wein F, Kaltenbacher M, Leugering G, Bänsch E, Schury F (2009a) Topology optimization of a piezoelectric-mechanical actuator with single- and multiple-frequency excitation. Int J Appl Electromagn Mech 30(3−4):201−221

Wein F, Kaltenbacher M, Schury F, Bänsch E, Leugering G (2009b) Topology optimization of a piezoelectric loudspeaker coupled with the acoustic domain. In: Proceedings WCSMO-08, 1−5 June 2009. Lisbon, Portugal

Wein F, Weller E, Albach T, Sutor A, Lerch R (2009c) Topology optimization of a piezoelectric energy harvester. In: Proceedings sensor 2009, vol II

Weller E (2009) Topology optimization of a piezoelectric energy harvester. Master's thesis, University of Erlangen-Nuremberg, Germany. In German

Zheng B, Chang CJ, Gea HC (2008) Topology optimization of energy harvesting devices using piezoelectric materials. Struct Multidisc Optim 38(1):17−23